ACS APPLIED ENERGY MATERIALS

Open Access

www.acsaem.org

Article

Enhanced Performance of a $Pr_4Ni_3O_{10\pm\delta}$–$Ce_{0.75}Gd_{0.1}Pr_{0.15}O_{2-\delta}$ Composite Electrode via Particle Size Grading

Zheng Xie, Yasmine Baghdadi, and Stephen J. Skinner*

Cite This: *ACS Appl. Energy Mater.* 2024, 7, 1640–1646

Read Online

ACCESS | Metrics & More | Article Recommendations | Supporting Information

ABSTRACT: A particle grading strategy was applied in $Pr_4Ni_3O_{10\pm\delta}$ (PNO)–$Ce_{0.75}Gd_{0.1}Pr_{0.15}O_{2-\delta}$ (CGPO) composite electrodes for intermediate-temperature solid oxide fuel cells. By testing of ungraded and graded electrodes and analysis of the obtained impedance spectra with the help of the distribution of relaxation time, it was found that the increase in oxygen species diffusion resistance, due to greater tortuosity of electrode particles, can be suppressed by the grading strategy. At the same time, the step of charge transfer can be enhanced. Overall, graded electrodes have much lower area specific resistance (ASR) than ungraded electrodes. The lowest ASR obtained for graded electrodes is 0.059 Ω cm^2 at 625 °C (0.025 Ω cm^2 at 698 °C) and p_{O_2} of 0.21 atm, nearly a one-fold decrease compared to 0.11 Ω cm^2 for ungraded electrodes at the same condition.

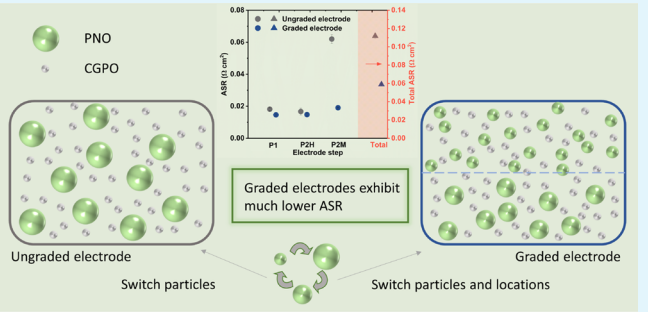

KEYWORDS: *Ruddlesden–Popper phase, composite electrode, layered electrode structure, low area specific resistance, DRT*

1. INTRODUCTION

Research has been focused on developing intermediate-temperature solid oxide fuel cells for higher durability, wider material selections, and lower manufacturing costs.[1−4] The main challenge in the electrode for operating in the intermediate temperature range (typically 600−700 °C) is the slow electrochemical kinetics such as the oxygen reduction reaction (ORR) in the cathode. To overcome this problem, a few strategies can be applied. A composite electrode consisting of ionic and electronic phases is an option because this extends the active area for electrochemical reactions from the interface between the electrode and electrolyte into the bulk of the electrode, enhancing the reaction kinetics.[5−7] Another option is applying innovative materials that exhibit mixed electronic and ionic conductivity.[8−10] This also helps to reduce the overpotential because the active area is the entire surface of the electrode. Both of these methods can be combined to increase the electrochemical reaction kinetics.

No matter what materials are selected as the electrode, the microstructure of the electrode is a key factor that determines the overpotential of the electrode. A typical electrode microstructure tailoring method is functionally grading the electrode. Many experiments were carried out to investigate how it helps to reduce the overpotential by particle size grading,[11,12] composition grading[7,11,13,14] and porosity grading.[15] Some simulation studies indicated that particle size grading is more advantageous than porosity grading at reducing the overpotential and a large particle size grading range is more effective than small ranges.[16,17]

In addition, it was reported that radical particle size grading should be cautiously considered in thin electrodes.[16,18]

This research was inspired by the idea of functional grading based on our previous research.[19] In the previous research, three composite electrodes composed of the same $Ce_{0.75}Gd_{0.1}Pr_{0.15}O_{2-\delta}$ (CGPO) and $Pr_4Ni_3O_{10\pm\delta}$ (PNO) with different particle sizes were investigated.[19] Regarding the role of these two materials, CGPO is an ionic conductor for extending the active area and PNO is a mixed ionic–electronic conductor and is electrochemically active for the ORR.[20−22] It was found that the smaller particles of the PNO phase reduced the area specific resistance (ASR) of charge transfer ($O_{ads} + 2e' + V_O^{\cdot\cdot} \rightarrow O_O^X$), but the conductivity of the composite was reduced. Therefore, it was of interest to investigate whether particle size grading can help to reduce the ASR of charge transfer without conductivity loss. Particle size grading was achieved by printing different electrode ink pastes alternatively: a layer attached to the interlayer and another layer on top of it. The only difference between the ink pastes was the particle size of the PNO phase.

Electrochemical impedance spectroscopy (EIS) was carried out to characterize the ASR of the symmetrical cells, and the distribution of relaxation time (DRT) was used to deconvolute

Received: December 15, 2023
Revised: January 18, 2024
Accepted: January 22, 2024
Published: February 13, 2024

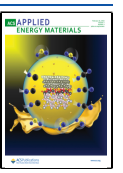

the impedance spectra to find the polarization resistances of all processes occurring in the electrode. The effect of particle size grading was discussed by observing how the ASR of each process changed with the electrode layout.

2. EXPERIMENTAL SECTION

PNO and CGPO powders were synthesized following the processes discussed in a previous work carried out by Xie et al. using a nitrate−citrate method.[19] CGPO powder was ready for the preparation of an electrode by this step, while further processes need to be carried out to obtain PNO powder. The product obtained after the nitrate−citrate method was calcined at 1050 °C under an oxygen flow for 12 h. This process was repeated seven times with grinding between each calcination.[20]

A planetary ball-mill instrument was used to crush the obtained PNO powder to produce smaller particles. A group of smaller particles was obtained by a set of milling agents, termed milled PNO. This milled PNO powder was milled further with another set of milling agents to achieve an even smaller particle size, termed twice-milled PNO.

The electrolyte pellets $Zr_{0.809}Sc_{0.182}Ce_{0.009}O_2$ (10Sc1CeSz) used in this study were commercial pellets (Lot No. 21AN02199, Kerafol, Germany) with a thickness of 150 ± 15 μm. A layer of 10Sc1CeSz was printed and sintered on each side of the pellet in order to increase the pellet surface roughness for better adhesion between the electrolyte and electrode. The 10Sc1CeSz powder (Lot No. H2228, DKKK, Japan) was mixed with a commercial ink vehicle (Fuel Cell Materials, USA, #311006) with a ratio of 1:1 wt % for the preparation of ink paste for interlayer deposition. The mixture was milled using a triple-roll mill to obtain a homogeneous distribution of powder in the ink vehicle. Meanwhile, the agglomerates of particles of each phase can be minimized because the distance between each roll was 5 μm.

The ink paste for electrode deposition was prepared by mixing CGPO powder, one type of PNO powder, and the ink vehicle with a ratio of 1:1:1 wt %. Also, the mixture was milled by triple-roll milling.

Electrode ink was deposited on the interlayer by screen printing. Particle size grading was achieved by printing different ink pastes alternatively. The notation of the cell is S^{XX}_{XX} in which the superscript represents a specific PNO phase with the CGPO phase on the top layer and the subscript represents a specific PNO phase with CGPO on the bottom layer. For instance, S^{MM}_{UM} is the cell that consists of unmilled PNO and CGPO on the bottom layer and twice-milled PNO and CGPO on the top layer. The printed electrode was sintered at 900 °C for 2 h with a heating and cooling rate of 2 °C/min. A layer of gold (Gwent Group, Code No. C2090908D1) was printed on the electrode as a current collecting layer followed by 2 h of sintering at 700 °C with a heating and cooling rate of 5 °C/min.

PNO powders with different processing histories, CGPO powder, and an electrolyte pellet with the interlayer deposited were characterized by X-ray diffraction (XRD; PANalytical X'Pert Pro MPD with a Cu Kα source) to identify their phase. In addition, electrodes were characterized to confirm the compatibility between the interlayer and electrode.

The electrode microstructures were characterized by focused-ion-beam scanning electron microscopy (FIB-SEM; Zeiss Auriga). The details of the quantitative analysis of the electrode microstructures were described in a previous work.[19]

The obtained three sets of PNO powders were characterized by a Brunauer−Emmett−Teller (BET) test (Micrometrics TriStar 3000) to identify their relative size by comparing their BET surface areas. The BET surface areas of different PNO powders were obtained via the BET equation. Nitrogen was used for the adsorption/desorption processes.

EIS with a frequency response analyzer (Solartron 1260a, AMETEK) was applied to characterize the symmetrical cells. The testing temperature ranged from 625 to 717 °C, and the atmosphere was controlled at p_{O_2} of 0.21 atm during EIS measurements.

3. RESULTS AND DISCUSSION

3.1. XRD. The materials used for constructing the symmetrical cells were characterized before preparation of the cells. The XRD patterns of unmilled PNO, milled PNO, and twice-milled PNO are given in Figure S1 and parts a and b of Figure S2, respectively. The XRD patterns of CGPO and the pellet attached with the interlayer are given in parts a and b of Figure S3, respectively. No signal from secondary phases was observed for each phase.

The XRD patterns of the electrodes are given in Figure S4. A secondary phase, NiO, was observed within the electrode. NiO was formed during electrode sintering at 900 °C. No additional NiO was formed during impedance measurements.[23]

3.2. BET. Different PNO powders were characterized by the BET test, and the BET surface area of each PNO powder is listed in Table 1. The result demonstrated that the planetary ball milling was effective in reducing the particle size of PNO powders. The particle size of twice-milled PNO was smaller than that of milled PNO, and the unmilled PNO was the largest. The isotherm linear plot and the BET surface area plot for three PNO powders are given in parts a and b of Figure S5, respectively.

Table 1. BET Surface Area of Different PNO Powders

PNO powder	unmilled	milled	twice-milled
BET surface area (m^2/g)	1.03 ± 0.01	7.19 ± 0.03	15.51 ± 0.08

3.3. Scanning Electron Microscopy (SEM). A SEM image of a cross section of a symmetrical cell is given in Figure 1a. A

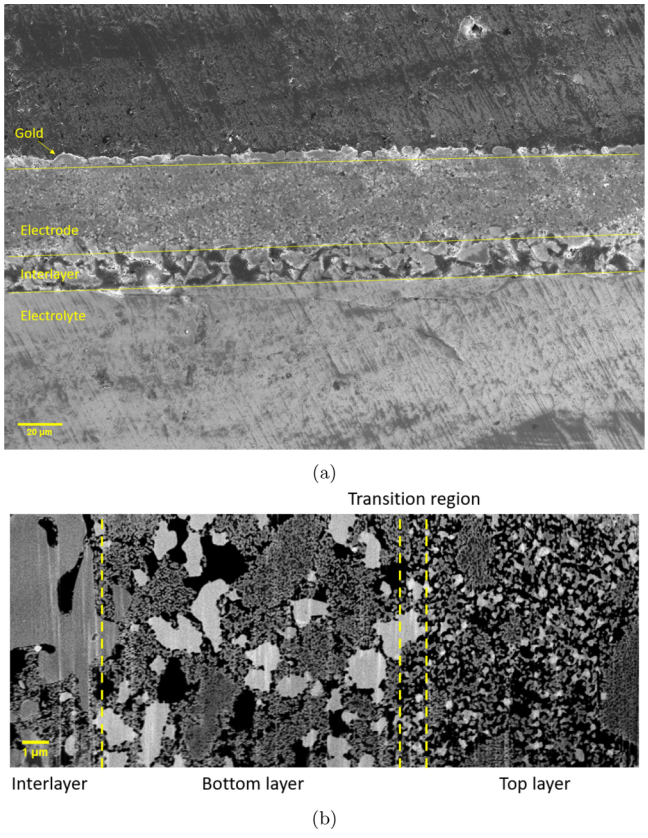

Figure 1. SEM images of cross sections of (a) a symmetrical cell and (b) a graded electrode of S^{MM}_{UM} in which the white, gray, and black phases represent PNO, CGPO, and a pores, respectively.

https://doi.org/10.1021/acsaem.3c03139
ACS Appl. Energy Mater. 2024, 7, 1640−1646

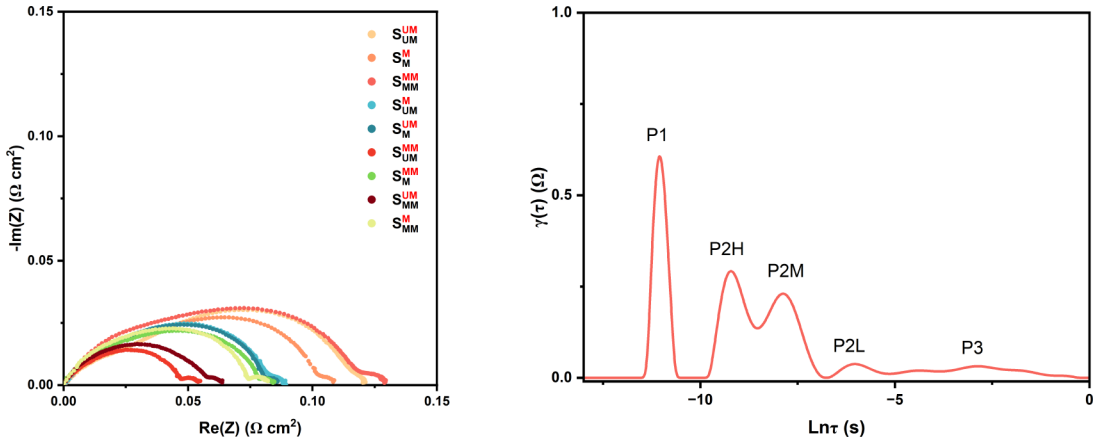

Figure 2. (a) Nyquist plot for all investigated symmetrical cells measured at 625 °C and p_{O_2} of 0.21 atm. (b) DRT spectrum for sample S^{MM}_{MM} measured at 625 °C and p_{O_2} of 0.21 atm, with regularization parameter λ of 10^{-4}.

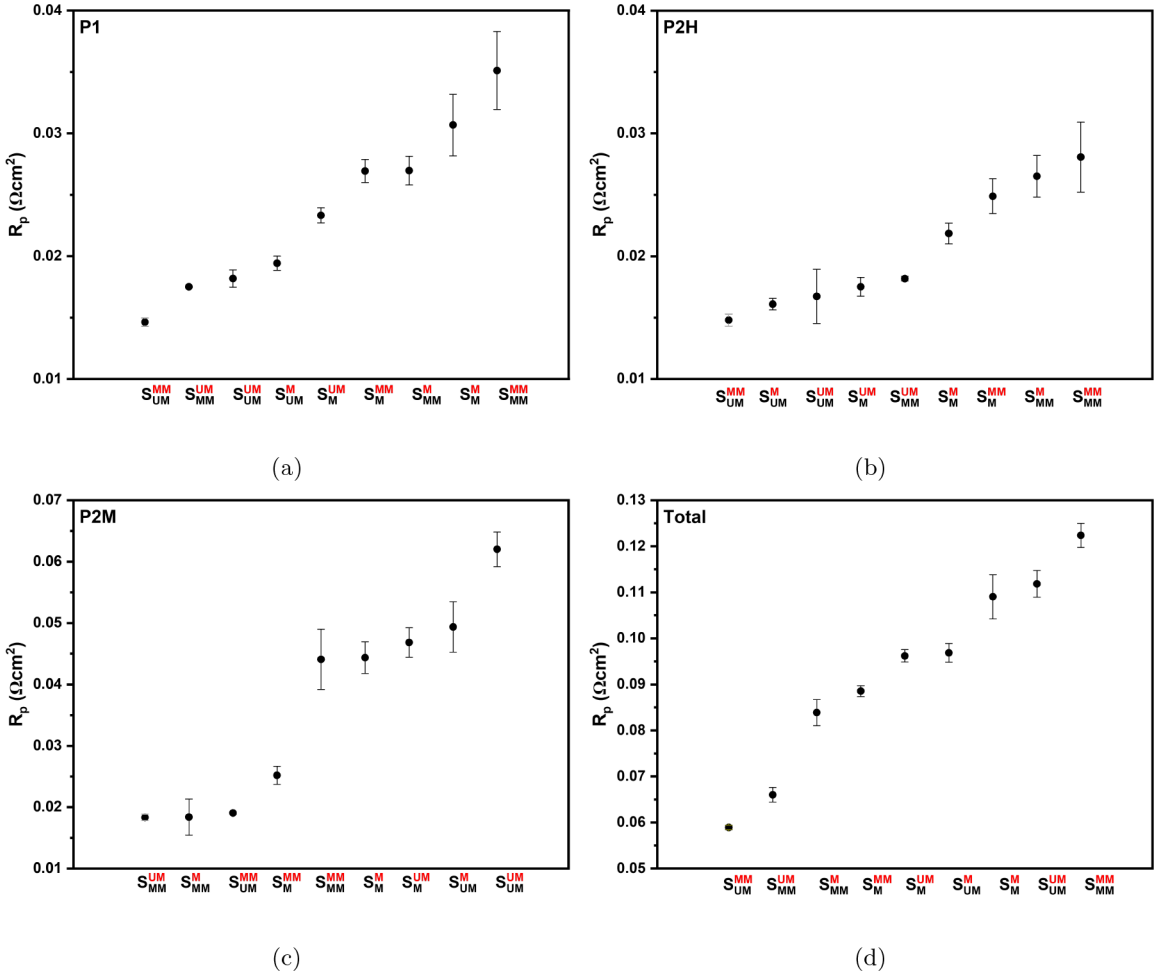

Figure 3. Polarization resistance of processes (a) P1, (b) P2H, and (c) P2M and (d) total resistance for all samples measured at 625 °C and p_{O_2} of 0.21 atm. The polarization resistance of each process ranged from small to large from the left to the right in each subfigure.

distinct layered structure in which a dense electrolyte is separated from the porous electrode by a porous interlayer with a thin layer of gold on top of the electrode surface can be observed.

The cross section of the electrode S^{MM}_{UM} was obtained by FIB-SEM, as shown in Figure 1b. Due to the porous nature of the electrode and interlayer, the bottom layer of the electrode partly penetrated into the interlayer and also the top layer of the

https://doi.org/10.1021/acsaem.3c03139
ACS Appl. Energy Mater. 2024, 7, 1640−1646

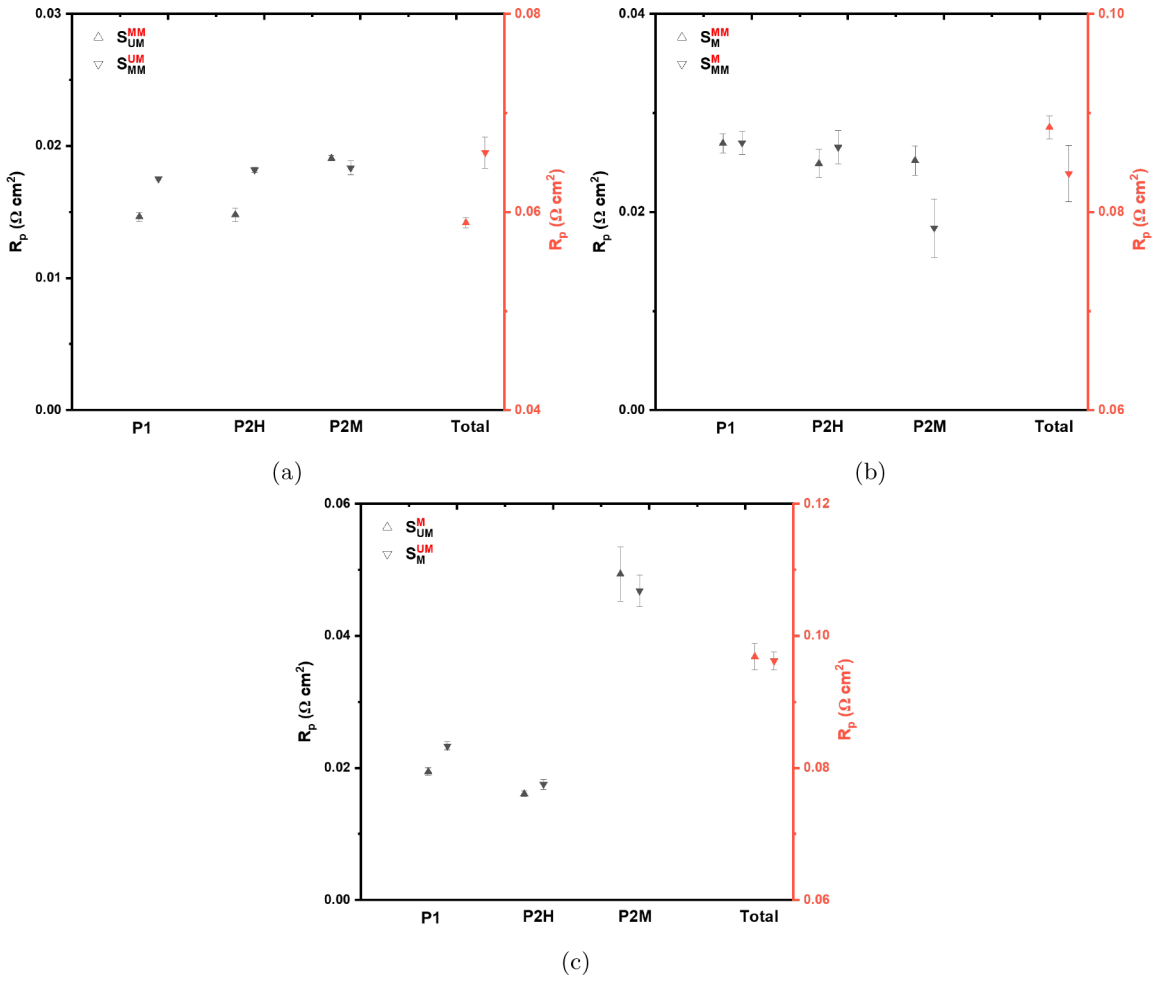

Figure 4. Polarization resistance of all processes and total polarization resistance for combinations between (a) unmilled and twice-milled PNO particles, (b) milled and twice-milled PNO particles, and (c) unmilled and milled PNO particles in electrodes measured at 625 °C and p_{O_2} of 0.21 atm.

electrode merged with the bottom layer of the electrode, forming a thin transition layer (typically around 1 μm).

The results of the quantitative analysis of electrodes without particle size grading are summarized in Table S1. They confirmed that the small PNO particles provide more active sites for the ORR. However, the tortuosity of PNO and CGPO increases, which accounts for the lower effective conductivity of PNO and CGPO.[24]

3.4. EIS. Each sample was characterized by EIS from 625 to 717 °C with an increment of around 20 °C at p_{O_2} of 0.21 atm. The Nyquist plot for all investigated samples measured at 625 °C is given in Figure 2a. The DRT was used to resolve the convoluted electrochemical processes that occurred within electrodes, and an example is given in Figure 2b. Five processes have been identified within the PNO−CGPO composite electrodes in a previous work.[19] It is reasonable to assume that these five processes still apply to the PNO−CGPO composite electrodes investigated here with additional particle-size-grading features. These five processes are as follows. (1) P1: oxygen-ion diffusion in the CGPO phase (ionic conductor). (2) P2H: oxygen incorporation at the PNO particle surface followed by diffusion in the PNO phase (a mixed ionic−electronic conductor and electrochemically active for the ORR). (3) P2M: charge transfer. (4) P2L: oxygen molecular dissociation. (5) P3: oxygen molecular adsorption.[19] In the following discussions, the processes P2L and P3 were less discussed because their resistance was virtually the same among all investigated cells, respectively, and the percentage of the sum of the resistances of P2L and P3 was low (around 12% in S^{MM}_{MM} and around 17% in S^{MM}_{UM}).

The DRT was applied to each sample to extract the polarization resistance of each process that occurred at 625 °C and p_{O_2} of 0.21 atm. The ASR of each process for all investigated symmetrical cells is illustrated in Figure 3 in ascending order. It can be observed that the cells that exhibited lower polarization resistances of the processes P1 and P2H were the cells composed of the unmilled PNO phase, especially when the unmilled PNO phase was on the bottom layer, as shown in Figure 3a,b. The cells composed of the twice-milled PNO exhibited higher polarization resistances of the processes P1 and P2H, especially when the twice-milled PNO was on the bottom layer. This phenomenon was completely opposite to the polarization resistance of the process P2M. The cells that involved the twice-milled PNO showed the lowest polarization resistance of the process P2M especially when the twice-milled PNO phase was on the bottom layer, as shown in Figure 3c. Higher polarization resistances were given by the cells composed of the unmilled PNO phase.

These results were expected: the composite electrode consisting of a PNO phase with a large particle size exhibited higher conductivity, while the amount of effective triple-phase boundary for the ORR was lower; on the contrary, the

https://doi.org/10.1021/acsaem.3c03139
ACS Appl. Energy Mater. 2024, 7, 1640−1646

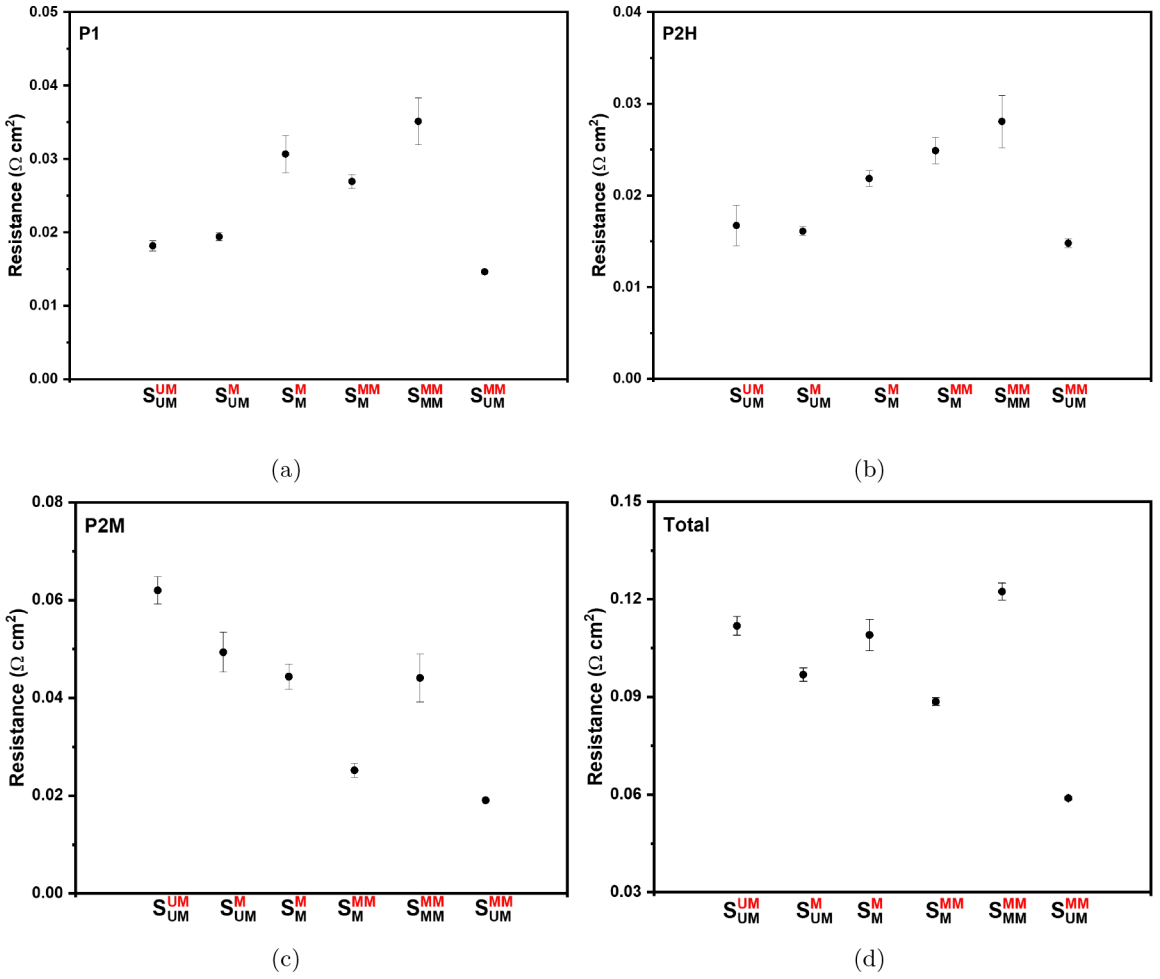

Figure 5. Polarization resistance of processes (a) P1, (b) P2H, and (c) P2M and (d) total resistance for three ungraded cells and three graded cells measured at 625 °C and p_{O_2} of 0.21 atm.

composite electrode consisting of a PNO phase with a smaller particle size exhibited lower conductivity but high ORR kinetics due to the increased amount of effective triple-phase boundary.[19] The microstructural data previously reported confirmed this finding and are provided in Table S1 and Figure S6 for convenience.[19] From Figure 3d, it can be observed that the nongraded cells S^{UM}_{UM}, S^{M}_{M}, and S^{MM}_{MM} exhibited the highest ASRs and the graded cells exhibited lower ASRs. This result demonstrated that electrode grading is an effective strategy to overcome the problem that a single PNO particle size cannot contribute to two aspects (conductivity and active area). In the following, it is necessary to establish how the electrode should be graded to achieve the lowest ASR.

The graded electrodes consisting of the same combination of PNO particles were compared to each other, as shown in Figure 4. It can be observed that the grading direction was less important because the polarization resistances of each process were very close to each other. Usually, particle size grading is designed as a configuration in which smaller electrode particles are on the bottom layer (electrolyte/electrode surface) and larger particles are on the top layer (free surface) in order to increase the active sites and simultaneously decrease the mass-transfer resistance.[16,17,25,26] However, such a configuration was not necessary for the composite electrodes investigated here. The reason could be that the composite electrodes were not suffering from concentration losses. Although there was not much difference in each step between graded electrodes with the same combination of PNO particles, as shown in Figure 4, there was an interesting result: the polarization resistances of P1 and P2H were always higher, and the polarization resistance of P2M was always lower when the smaller PNO particles were close to the electrolyte. When the larger PNO particles were close to the electrolyte, the polarization resistances of P1 and P2H were lower and that of P2M was higher. This was sensible because the electrode reaction mainly occurs close to the electrolyte, as confirmed by many simulation reports.[18,27−29] Hence, the corresponding advantage of the particle close to the electrolyte was greater. Because the size-grading direction was less important, for the sake of simplicity, one graded electrode from different combinations was selected to investigate. Therefore, the polarization resistances of three cells without particle size grading and three cells with particle size grading were compared for each process, as shown in Figure 5.

From Figure 5a,b, it can be observed that when S^{UM}_{UM} was modified to S^{M}_{M} and then to S^{MM}_{MM} or S^{UM}_{UM} was directly modified to S^{MM}_{MM}, for increasing active sites without particles size grading, the polarization resistances of processes P1 and P2H increased steadily. However, if the particle size was only decreased in one layer, i.e., applying particle size grading, the polarization resistance of P1 decreased and the polarization resistance of P2H maintained the original value. A possibility was that the

https://doi.org/10.1021/acsaem.3c03139
ACS Appl. Energy Mater. 2024, 7, 1640−1646

transition region identified in Figure 1b enhanced the electrode conductivity.

The polarization resistance of process P2M decreased from 0.062 Ω cm^2 for S^{UM}_{UM} to 0.044 Ω cm^2 for S^{M}_{M}, but no further decrease was observed for S^{MM}_{MM}, although it was expected to give a lower polarization resistance because it had the greatest active area. This was explained by the large polarization resistance of processes P1 and P2H for S^{MM}_{MM}, which limited ion migration from the electrode to the electrolyte and then restricted process P2M because the aggregation of oxygen ions at the interface between the electrode and electrolyte resisted the oxygen ions.[30] With particle size grading, the polarization resistance was significantly reduced to 0.025 Ω cm^2 for S^{MM}_{M} and 0.019 Ω cm^2 for S^{MM}_{UM}. This improvement was ascribed to the smaller polarization resistance of processes P1 and P2H, which activated the active area within the electrode layer in which twice-milled PNO particles were present. The polarization resistance of process P2M of the graded cell S^{M}_{UM} was 0.049 Ω cm^2, which was between that of S^{UM}_{UM} and S^{M}_{M}. This was reasonable, and the active site in S^{M}_{UM} was functioning because the average particle size of S^{M}_{UM} was somewhere between those of S^{UM}_{UM} and S^{M}_{M}. Therefore, to obtain a lower polarization resistance, the smaller particles should be used to provide more active sites.

The graded electrodes exhibited lower polarization resistance than ungraded electrodes, as shown in Figure 5d. The lower total polarization resistance of graded S^{M}_{UM} of 0.097 Ω cm^2 was attributed to the lower polarization resistance of P2M thanks to the presence of a layer of milled PNO particles without an increase in the polarization resistance of processes P1 and P2H. For the graded S^{MM}_{M}, the polarization resistance of P2M was further decreased due to a layer of twice-milled PNO particles, which provided the greatest amount of active sites. However, the average particle size of the graded S^{MM}_{M} was relatively small, which resulted in the greatest polarization resistance of processes P1 and P2H among the graded electrodes. Hence, its total polarization resistance of 0.088 Ω cm^2 was the second lowest. The lowest total polarization resistance was given by S^{MM}_{UM} of 0.059 Ω cm^2 for two reasons. The first reason is that the presence of one layer of electrode consisting of twice-milled PNO particles provided the greatest amount of active sites and hence the lowest P2. The second reason is that the presence of one layer of electrode composed of unmilled PNO particles enabled the low polarization resistance of processes P1 and P2H and maximized the functionality of active sites within the layer composed of twice-milled PNO particles.

The Arrhenius plot of the total polarization resistance of the electrode S^{MM}_{UM} was given in Figure S12. The ASRs of commonly investigated cathodes are summarized in Table 2. To our knowledge, there is only one research on PNO in the literature in which the single-phase PNO was applied as the electrode material.[35] Compared to the single-phase PNO electrode, the introduction of CGPO forming a composite electrode effectively reduced the ASR of the electrode. With further electrode optimization, i.e., particle size grading forming a layered electrode structure, the ASR is much lower than the value reported in ref 35. The composite electrode with particle size grading investigated here also exhibited a strong competitive performance compared to other commonly investigated cathode materials.

4. CONCLUSIONS

In conclusion, particle size grading was effective in reducing the total resistance by combining the advantages of different PNO particles. Particle size grading was less important in this composite because the diffusion resistance was minor. The combination of different PNO particles was more important and determined the total resistance of the graded electrode. Among the graded electrodes, the combination of unmilled and milled particles was short of active area, which resulted in a less competitive resistance of process P2M. The combination of milled and twice-milled PNO particles had an abundant active area. However, the small PNO particles led to higher resistance of processes P1 and P2H, which also to some extent impeded process P2M. The combination of unmilled and twice-milled PNO was the best combination because the presence of twice-milled PNO provided enough active area, and the presence of unmilled PNO not only enabled low resistance of processes P1 and P2H but also maximized the functionality of the active area provided by twice-milled PNO.

Table 2. Polarization Resistance Comparison with Commonly Investigated Cathode Materials

cathode	temperature (°C)	R_p (Ω cm^2)	ref
$Pr_4Ni_3O_{10\pm\delta}$ + $Ce_{0.75}Gd_{0.1}Pr_{0.15}O_{2-\delta}$	625/698	0.059/0.025	present work
$La_2NiO_{4+\delta}$ + $Ce_{0.9}Gd_{0.1}O_{1.95}$	600	0.15	31
$Pr_2NiO_{4+\delta}$ + $Ce_{0.8}Gd_{0.2}O_{1.90}$	600	0.075	32
triple-layer $La_2NiO_{4+\delta}$	600	0.16	33
triple-layer $Pr_2NiO_{4+\delta}$	600	0.04	33
$La_3Ni_2O_{7+\delta}$ + $Ce_{0.9}Gd_{0.1}O_{2-\delta}$	600	0.13	34
$Pr_4Ni_3O_{10+\delta}$	600	0.16	35
$La_{0.58}Sr_{0.4}Co_{0.2}Fe_{0.8}O_{3-\delta}$	700	0.1	36
$La_{0.8}Sr_{0.2}MnO_3$ + $La_{0.58}Sr_{0.4}Co_{0.2}Fe_{0.8}O_{3-\delta}$	700	0.08	36
$La_{0.6}Sr_{0.4}CoO_{3-\delta}$ + $La_{0.58}Sr_{0.4}Co_{0.2}Fe_{0.8}O_{3-\delta}$	700	0.08	36

■ ASSOCIATED CONTENT

Data Availability Statement

The original EIS and DRT data are available in Zenodo (https://zenodo.org/communities/electroceramic-materials/).

Supporting Information

The Supporting Information is available free of charge at https://pubs.acs.org/doi/10.1021/acsaem.3c03139.

Additional experimental results, including XRD data for the PNO and CGPO phases and electrodes, BET data for PNO, microstructural data from FIB-SEM, 3D rendering data, particle size distribution data, EIS and DRT data, and polarization resistance of electrodes (PDF)

■ AUTHOR INFORMATION

Corresponding Author

Stephen J. Skinner − *Department of Materials, Imperial College London, London SW7 2AZ, U.K.; International Institute for Carbon Neutral Energy Research, Kyushu University, Nishi-ku, Fukuoka 819-0395, Japan;* orcid.org/0000-0001-5446-2647; Phone: +44 (0)20 7594 6782; Email: s.skinner@imperial.ac.uk

Authors

Zheng Xie − *Department of Materials, Imperial College London, London SW7 2AZ, U.K.*

Yasmine Baghdadi − *Department of Chemical Engineering, Imperial College London, London SW7 2AZ, U.K.;* orcid.org/0000-0002-0143-2572

https://doi.org/10.1021/acsaem.3c03139
ACS Appl. Energy Mater. 2024, 7, 1640−1646

Complete contact information is available at:
https://pubs.acs.org/10.1021/acsaem.3c03139

Notes

The authors declare no competing financial interest.

■ ACKNOWLEDGMENTS

The authors thank Dr. Salvador Eslava for access to the BET instrument in the Chemical Engineering Department, Imperial College London. S.J.S. thanks the Royal Academy of Engineering for the award of a Research Chair (RCSRF2021\1243).

■ REFERENCES

(1) Fergus, J. *Materials Science and Engineering: A* **2005**, *397*, 271−283.
(2) Tietz, F.; Buchkremer, H.-P.; Stöver, D. *Solid State Ionics* **2002**, *152−153*, 373−381.
(3) Menzler, N.; Tietz, F.; Uhlenbruck, S.; Buchkremer, H.; Stöver, D. *J. Mater. Sci.* **2010**, *45*, 3109−3135.
(4) Orera, A.; Slater, P. R. *Chem. Mater.* **2010**, *22*, 675−690.
(5) Kenjo, T.; Nishiya, M. *Solid State Ionics* **1992**, *57*, 295−302.
(6) Kenjo, T.; Osawa, S.; Fujikawa, K. *J. Electrochem. Soc.* **1991**, *138*, 349−355.
(7) Woolley, R.; Skinner, S. *Solid State Ionics* **2014**, *255*, 1−5.
(8) Chroneos, A.; Vovk, R.; Goulatis, I.; Goulatis, L. *J. Alloys Compd.* **2010**, *494*, 190−195.
(9) Sun, C.; Hui, R.; Roller, J. *J. Solid State Electrochem.* **2010**, *14*, 1125−1144.
(10) Tarancón, A.; Burriel, M.; Santiso, J.; Skinner, S.; Kilner, J. *J. Mater. Chem.* **2010**, *20*, 3799−3813.
(11) Liu, Y.; Compson, C.; Liu, M. *J. Power Sources* **2004**, *138*, 194−198.
(12) Liu, Z.; Liu, M.; Nie, L.; Liu, M. *Int. J. Hydrogen Energy* **2013**, *38*, 1082−1087.
(13) Fontaine, M.; Laberty-Robert, C.; Ansart, F.; Tailhades, P. *J. Power Sources* **2006**, *156*, 33−38.
(14) Zha, S.; Zhang, Y.; Liu, M. *Solid State Ionics* **2005**, *176*, 25−31.
(15) Holtappels, P.; Sorof, C.; Verbraeken, M. C.; Rambert, S.; Vogt, U. *Fuel Cells* **2006**, *6*, 113−116.
(16) Ni, M.; Leung, M.; Leung, D. *J. Power Sources* **2007**, *168*, 369−378.
(17) Liu, L.; Flesner, R.; Kim, G.-Y.; Chandra, A. *Fuel Cells* **2012**, *12*, 97−108.
(18) Wang, C. A Computational Analysis of Functionally Graded Anode in Solid Oxide Fuel Cell by Involving the Correlations of Microstructural Parameters. *Energies* **2016**, *9*, 408.
(19) Xie, Z.; Jang, I.; Ouyang, M.; Hankin, A.; Skinner, S. *Journal of Physics: Energy* **2023**, *5*, No. 045005.
(20) Tsai, C.-Y.; Aguadero, A.; Skinner, S. *J. Solid State Chem.* **2020**, *289*, No. 121533.
(21) Bassat, J.; Allançon, C.; Odier, P.; Loup, J.; Carvalho, M. D.; Wattiaux, A. *European Journal of Solid State and Inorganic Chemistry* **1998**, *35*, 173−188.
(22) Cheng, S.; Chatzichristodoulou, C.; Søgaard, M.; Kaiser, A.; Hendriksen, P. *J. Electrochem. Soc.* **2017**, *164*, F1354−F1367.
(23) Tsai, C. Phase evolution and reactivity of $Pr_2NiO_{4+\delta}$ and $Ce_{0.9}Gd_{0.1}O_{2-\delta}$ solid oxide cell electrodes. Ph.D. Thesis, Imperial College London, London, U.K., 2020.
(24) Atkinson, A.; Baron, S.; Brandon, N. *J. Electrochem. Soc.* **2004**, *151*, No. E186.
(25) Yan, Z.; He, A.; Hara, S.; Shikazono, N. *Int. J. Hydrogen Energy* **2022**, *47*, 16610−16625.
(26) Shi, J.; Xue, X. *J. Electrochem. Soc.* **2011**, *158*, B143.
(27) Ji, Y.; Yuan, K.; Chung, J. *J. Power Sources* **2007**, *165*, 774−785.
(28) Chan, S. H.; Chen, X. J.; Khor, K. A. *J. Electrochem. Soc.* **2004**, *151*, A164.
(29) Chen, X.; Chan, S.; Khor, K. *Electrochim. Acta* **2004**, *49*, 1851−1861.
(30) Hildenbrand, N.; Nammensma, P.; Blank, D.; Bouwmeester, H.; Boukamp, B. *J. Power Sources* **2013**, *238*, 442−453.
(31) Nicollet, C.; Flura, A.; Vibhu, V.; Rougier, A.; Bassat, J.; Grenier, J. *J. Power Sources* **2015**, *294*, 473−482.
(32) Nicollet, C.; Flura, A.; Vibhu, V.; Fourcade, S.; Rougier, A.; Bassat, J.; Grenier, J. *J. Solid State Electrochem.* **2016**, *20*, 2071−2078.
(33) Sharma, R.; Burriel, M.; Dessemond, L.; Bassat, J. M.; Djurado, E. *Journal of Material Chemistry A* **2016**, *4*, 12451−12462.
(34) Sharma, R.; Burriel, M.; Dessemond, L.; Bassat, J.; Djurado, E. *J. Power Sources* **2016**, *325*, 337−345.
(35) Vibhu, V.; Rougier, A.; Nicollet, C.; Flura, A.; Fourcade, S.; Penin, N.; Grenier, J.; Bassat, J. *J. Power Sources* **2016**, *317*, 184−193.
(36) Vibhu, V.; Yildiz, S.; Vinke, I. C.; Eichel, R.-A.; Bassat, J.-M.; de Haart, L. G. *J. Journal of The Electrochemical Society* **2019**, *166*, F102.